

Observation of Transient Parity-Time Symmetry in Electronic Systems

Xin Yang¹, Jiawen Li¹, Yifei Ding^{1,*}, Mengwei Xu¹, Xue-Feng Zhu^{2,†} and Jie Zhu^{3,4,‡}

¹College of Electrical and Information Engineering, National Electric Power Conversion and Control Engineering Technology Research Center, Hunan University, Changsha, Hunan 410082, People's Republic of China

²School of Physics, Huazhong University of Science and Technology, Wuhan, Hubei 430074, People's Republic of China

³School of Physics Science and Engineering, Tongji University, Shanghai 200092, People's Republic of China

⁴Shanghai Research Institute for Intelligent Autonomous Systems, Tongji University, Shanghai 201210, People's Republic of China

 (Received 30 May 2021; accepted 13 January 2022; published 10 February 2022)

We demonstrate the transient parity-time (PT) symmetry in electronics. It is revealed by equivalent circuit transformation according to the switching states of electronic systems. With the phasor method and Laplace transformation, we derive the hidden PT-symmetric Hamiltonian in the switching oscillation, which are characterized by free oscillation modes. Both spectral and dynamic properties of the PT electronic structure demonstrate the phase transition with eigenmode orthogonality. Importantly, the observed transient PT symmetry enables exceptional-point-induced optimal switching oscillation suppression, which shows the significance of PT symmetry in electronic systems with temporary responses. Our work paves the way for breakthroughs in the PT symmetry theory and has essential applications such as anti-interference in switch-mode electronics.

DOI: [10.1103/PhysRevLett.128.065701](https://doi.org/10.1103/PhysRevLett.128.065701)

Parity-time (PT) symmetric Hamiltonians, as a class of non-Hermitian Hamiltonians, have attracted intense interest due to the property of phase transition and entirely real spectrum [1]. In the past decade, many studies have demonstrated the PT symmetry in photonics [2–4], electronics [5–10], and acoustics [11–13]. Rapid development of creating and understanding PT-symmetric structures has led to various nontrivial features, such as unidirectional invisibility [14], invisible sensing [12], single-mode lasing [15], sensitive readout [8], and robust wireless power transfer [6]. However, the stringent requirement to build gain has hindered the possibilities to verify and implement these concepts in practical devices. Therefore, a gain-free route to PT symmetry has been introduced which captured great research interests [16–21]. For example, a class of simple Hamiltonians comprising two dissipative components were constructed, where hidden PT symmetry is revealed after a gauge transformation [2]. Multilayered structures of hidden PT symmetry have been widely studied in photonics and acoustics, revealing that in passive systems an exceptional point (EP) and its associated phase transition can be measurable quantities and featured with unidirectional responses [22,23].

In electronics, PT-symmetric circuits at the steady state [24–26] were intensely investigated, such as robust wireless power transfer [6–10]. However, the exploration on PT symmetry in the widely existing transients of electronic systems is still elusive, which is nonetheless significant for both theories and applications. In recent years, the advent of wideband gap semiconductor switch devices has been

revolutionizing power electronics. Because of unique merits including lower loss, higher power density, and better thermal performance, they have become promising alternatives of silicon switch devices for higher efficiency and higher power density applications. However, a big challenge of severe switching oscillation exists for their efficient and reliable applications, which is mainly excited by ultrafast switching and caused by low on-state loss, inevitably leading to the severe electromagnetic interference, additional oscillation losses, and system breakdown by wrongly triggered switching [27–29].

In this Letter, we propose an electronic structure that has the transient PT symmetry triggered by the switching on and off of electronic devices and provides an intriguing solution to release the unwanted oscillation energy triggered by fast switching. The electronic structure of the transient PT symmetry is constructed by inductively coupling a secondary circuit to a switch-mode primary circuit to form a pair of gainless dimers. These unique dimer structures are derived by equivalent circuit transformation and simplification according to the switching states of electronic systems. The rapid switching of electronic devices provides an initial condition for the passive dimers to reveal the hidden PT symmetry. It is essentially different from previous works where the passive optical system requires sophisticated preexcitations [16]. On the basis of the phasor method and the Laplace transformation, our scheme not only probes the spectral and dynamic properties of electronic systems with a hidden transient PT symmetry, but also demonstrates loss-tuned

optimal damping while still maintaining the very low lossy state of the primary side at the EP. That is very conducive to solving the critical issues of advanced wide-band-gap semiconductor switch devices in real applications.

Distinctive from conventional damping techniques of directly introducing physical loss elements at the primary-side switch-mode circuit [28,29], our proposed method, provided by transient PT symmetry, proposes an indirect solution to damping the unwanted oscillation energy. A “virtual” lossy element is established to the primary switch-mode loop. Losses to damp the switching oscillation at the primary side are almost transferred to the secondary oscillator. Additionally, little impact can be made to the original primary side by a low coupling strength.

A PT-symmetric dimer normally consists of a balanced gain and loss. Figure 1(a) displays a PT-symmetric dimer under the forced oscillation mode of $Ae^{i\omega t}$. It is under a steady-state condition and adopts the identical LC circuits in Fig. 1(b) [6–10]. In Figs. 1(c) and 1(d), the concept of transient PT symmetry is proposed. It is triggered by switching on and off of electronic devices. After the rapid switching process, transients of parasitic elements in the circuit are established at the start of on- and off-states, which can be described by the free oscillation transient mode of $Ae^{(i\omega-\gamma)t}$. Furthermore, this transient PT-symmetric circuit has a more flexible configuration without requiring identical LC resonators [see Fig. 1(d)]. The dimer consists of asymmetric lossy sites without the need for an active gain, so that its stability can be easily ensured

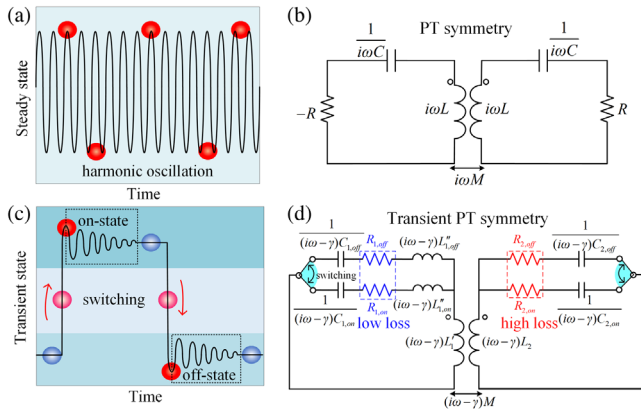


FIG. 1. (a) The steady electronic system under the time-harmonic state, which can be an active PT-symmetric dimer denoted by the red spheres. (b) A PT-symmetric circuit under the forced oscillation mode of $Ae^{i\omega t}$. (c) The transient electronic system under the switching state over time. Only for transients at the start of on- and off-state, the electronic system is equivalent to a passive PT dimer, indicating the existence of transient PT symmetry. The color change from blue spheres to red spheres indicates the energy increase. (d) The proposed transient PT-symmetric circuits which are established at the start of on- and off-states under the free oscillation mode of $Ae^{(i\omega-\gamma)t}$ in the switching process.

[2,7,16]. These free oscillation phenomena, such as transient currents, charges, discharges, or temporary disturbances are very common in electronics [30–33]. By the phasor method using complex angular velocities, the impedance of an inductor becomes $(i\omega - \gamma)L$, the impedance of a capacitor becomes $1/[(i\omega - \gamma)C]$, and the circuit current is $Ae^{(i\omega-\gamma)t}$, with the resistance R being unchanged in Fig. 1(d) [34,35]. This method can transform the transient circuit analysis into an analogous “steady-state” circuit analysis.

Figure 2(a) schematically depicts the circuit diagram of the switch-mode circuit at the primary side with a wirelessly coupled PCB circuit at the secondary side. A typical switch-mode cell at the primary side is mainly composed of a SiC MOSFET, a SiC diode, a dc voltage source and an inductive load. The on-state losses of both devices are very small while the off-state losses are negligible. In addition, their switching speed is ultrafast so that their switching loss is very low (tens of microjoules). Therefore, in terms of the losses, this switch-mode excitation is more efficient than the conventional operational amplifiers [6,7]. The secondary oscillator is composed of a printed circuit board (PCB) with coupling coils, capacitors, and resistors connected in series. We choose a physically asymmetric design that the secondary inductance is an order of magnitude larger than the total primary inductance to increase the inductive coupling coefficient. Further, our coupling fashion can minimize the parasitic inductance influence to the primary oscillator [36], which is significant for practical system design and implementation.

Our proposed transient PT-symmetric dimer is not directly composed of the steady RLC circuit, but an equivalent circuit of a switch-mode electronic converter derived according to the switching states of electronic

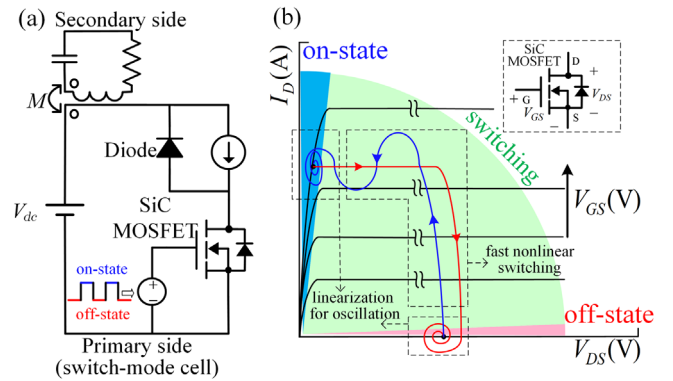


FIG. 2. (a) Circuit diagram of the primary-side switch-mode circuit with a wirelessly coupled PCB circuit. The secondary circuit is coupled to the primary circuit. (b) The output curves of SiC MOSFET. I_D is the drain current of the MOSFET that is the primary-side current, V_{DS} is the drain to source voltage and V_{GS} is the gate voltage. The MOSFET full switching process is a typical nonlinear switching trajectory (blue trace: turn-on; red trace: turn-off).

devices. For the primary switch-mode circuit, a gate signal controls SiC MOSFET to switch on and off. Figure 2(b) shows the output characteristic curves of SiC MOSFET. The switching process can be depicted into a typical nonlinear switching trajectory, viz., the blue and red curves in Fig. 2(b). The green area is the “saturation” region for MOSFET. The quick switching behavior mainly in the green area excites free oscillation after the SiC MOSFET switching has been completed [27–30]. Here, we focus on the oscillation process. For the on- and off-states of SiC MOSFET, two different linearized equivalent circuits can be simplified and derived. When the MOSFET is at on-state with a very low $R_{DS,on}$, the diode is off-state and acts as a capacitor C_J . Conversely, when the MOSFET is off-state, the diode is at on-state and acts as a low resistor $R_{diode(on)}$. Therefore, a pair of different equivalent RLC oscillators at both turn-on and turn-off oscillations can be derived after a series of circuit simplification and transformation in Fig. 1(d) [36].

We combine the phasor method and the Laplace transformation to reveal the transient PT symmetry in electronic systems with free oscillation modes. The coupling-mode equations of the circuit under free oscillations in Fig. 1(d) are derived as

$$\begin{pmatrix} U_1 \\ U_2 \end{pmatrix} = (i\omega - \gamma) \begin{pmatrix} L_1 & M \\ M & L_2 \end{pmatrix} \begin{pmatrix} I_1 \\ I_2 \end{pmatrix}. \quad (1)$$

Applying Kirchoff’s voltage law, we also have

$$\begin{aligned} U_1 + R_1 I_1 + \frac{I_1}{(i\omega - \gamma)C_1} &= 0, \\ U_2 + R_2 I_2 + \frac{I_2}{(i\omega - \gamma)C_2} &= 0, \end{aligned} \quad (2)$$

where U_n and I_n denote the voltage and the current through inductors, respectively. With $\{[(\omega + i\gamma)^2 - \omega_n^2]/[2(\omega + i\gamma)]\} \approx \omega + i\gamma - \omega_n$, by combining Eqs. (1) and (2), we obtain

$$\begin{pmatrix} i(\omega_1 - \omega - i\gamma) - \gamma_1 & i\kappa \\ i\kappa & i(\omega_2 - \omega - i\gamma) - \gamma_2 \end{pmatrix} \begin{pmatrix} a_1 \\ a_2 \end{pmatrix} = 0, \quad (3)$$

where $a_n = \sqrt{(L_n/2)}I_n$ is proportional to the inductance current and $|a_n|^2$ is the energy stored in the inductor. We also have the resonance frequency $\omega_n = (1/\sqrt{L_n C_n})$, loss rate $\gamma_n = (R_n/2L_n)$, coupling rate $\kappa = -[(\omega + i\gamma)\mu/2]$, and coupling coefficient $\mu = (M/\sqrt{L_1 L_2})$. In a passive system under free oscillation modes, ω is usually much larger than γ , and thus we assume that $\kappa \approx -(\omega\mu/2)$. Considering the free oscillation currents $a_n(t) \rightarrow a_n e^{(i\omega - \gamma)t}$, the time evolution of the amplitudes of oscillators $a[a_1, a_2]$ can be described by the following equation:

$$-i \frac{d}{dt} \begin{pmatrix} a_1 \\ a_2 \end{pmatrix} = \underbrace{\begin{pmatrix} \omega_1 + i\gamma_1 & \kappa \\ \kappa & \omega_2 + i\gamma_2 \end{pmatrix}}_H \begin{pmatrix} a_1 \\ a_2 \end{pmatrix}, \quad (4)$$

where H is a non-Hermitian Hamiltonian. We define $\chi = [(\gamma_1 + \gamma_2)/2]$ and apply the gauge transformation $[a_1, a_2] = e^{-\chi t} [A_1, A_2]$, and the PT symmetry can be reestablished as

$$-i \frac{d}{dt} \begin{pmatrix} A_1 \\ A_2 \end{pmatrix} = \underbrace{\begin{pmatrix} \omega_1 - i\frac{\gamma_2 - \gamma_1}{2} & \kappa \\ \kappa & \omega_2 + i\frac{\gamma_2 - \gamma_1}{2} \end{pmatrix}}_{H'} \begin{pmatrix} A_1 \\ A_2 \end{pmatrix}. \quad (5)$$

The new Hamiltonian H' in Eq. (5) has the same off-diagonal elements κ as the original Hamiltonian H , but the imaginary parts of diagonal elements are now balanced. This system can be identified as a passive system with the transient PT symmetry, since $[H', PT] = 0$ is satisfied. We only need $\omega_1 = \omega_2$ to guarantee the PT symmetry of H' . Therefore, the transient PT-symmetric structure can have a very flexible configuration, for example comprising different LC oscillators ($L_1 \neq L_2$).

Eigenvalues of the transformed Hamiltonian H' are $\lambda_{1,2} = \omega_0 \pm \sqrt{\kappa^2 - (\gamma_2 - \gamma_1)^2/4}$. Here, we define $\Delta = \kappa^2 - (\gamma_2 - \gamma_1)^2/4$. The evolutions of two eigenmodes $|1\rangle \exp(i\sqrt{\Delta}t)$ and $|2\rangle \exp(-i\sqrt{\Delta}t)$ are given in the form of sinusoidal or exponential functions. When $\Delta > 0$, the two eigenmodes $|1\rangle \exp(i\sqrt{\Delta}t)$ and $|2\rangle \exp(-i\sqrt{\Delta}t)$ are sinusoidal functions. At $\Delta = 0$, the eigenmodes coalesce and the system operates at an EP. In this case, spontaneous PT symmetry breaking occurs at $\gamma_2 = -2\kappa + \gamma_1$, marking the onset of phase transition. As γ_2 further grows, $\sqrt{\Delta}$ becomes a complex number and the two eigenvalues become a complex conjugate pair in the broken PT phase. The eigenmodes transform into exponential functions with one growing and the other decaying. The eigenvalues of Hamiltonian H are $\lambda_{1,2} = \omega_0 + i[(\gamma_1 + \gamma_2)/2] \pm \sqrt{\kappa^2 - [(\gamma_2 - \gamma_1)^2/4]}$. Comparing with H' after gauge transformation, the system described by H has a larger loss rate of $[(\gamma_1 + \gamma_2)/2]$. This loss rate reflects a hyperbolic angular velocity, which causes the circuit modes to attenuate and freely oscillate. In the broken phase, the two modes decay at different rates, indicating loss rate splitting.

We conduct experiments to study spectral properties of the transient PT symmetry in the proposed electronic system [36]. The advanced particle swarm optimization (PSO) algorithm [37,38] is used to accurately fit measured results of the free oscillating currents in the primary oscillator to yield the loss rates and the frequencies, which is difficult to be observed directly from the raw experimental results. The indicators identified by PSO are beneficial to reveal and reflect the characteristic of transient PT symmetry. $I_1(t) = e^{-\text{Im}(\lambda_0)(t+t_0)} \{C_1 \cos[\text{Re}(\lambda_1)(t+t_0)] + C_2 \cos[\text{Re}(\lambda_2)(t+t_0)]\}$ and $I_2(t) = \cos[\text{Re}(\lambda_0)(t+t_0)] \times [C_1 e^{-\text{Im}(\lambda_1)(t+t_0)} + C_2 e^{-\text{Im}(\lambda_2)(t+t_0)}]$ are the objective functions in the symmetric and broken phases, respectively.

Here, $\text{Im}(\lambda_0)$ is the loss rate of eigenmodes in the symmetric phase. $\text{Re}(\lambda_1)$ and $\text{Re}(\lambda_2)$ are the frequencies of the eigenmodes in the exact PT-symmetry phase. $\text{Re}(\lambda_0)$ is the frequency in the broken phase. $\text{Im}(\lambda_1)$ and $\text{Im}(\lambda_2)$ are the loss rates in the broken phase. $C_{1,2}$ is the initial amplitude. Since we only analyze the transient oscillation processes, we use t_0 as a variable to compensate for the time delay. The results are compared with the eigenvalues of H in Eq. (4) [see Figs. 3(a) and 3(c)]. In order to prove the accuracy of the proposed equation to find the EP analytically, more experimental data around the EP are added to demonstrate the distinctive phase characteristics. Here, the secondary resistance R_2 is used to tune the loss rate γ_2 . $\text{Re}(\lambda)$ represents the frequencies of the two modes while $\text{Im}(\lambda)$ represents the loss rates. The experimental results nicely agree with the theoretical results proposed above and demonstrate the hidden PT symmetry behaviors in the proposed system.

The eigenvector can be obtained from the Hamiltonian H' [36]. In the PT-symmetric phase, the eigenvector is $|\lambda_1, \lambda_2\rangle = (1, \mp e^{\pm i\varphi})^T$, where $\sin \varphi = [(\gamma_2 - \gamma_1)/(-2\kappa)]$. When the system enters the broken phase, the eigenvector is $|\lambda_1, \lambda_2\rangle = (1, -ie^{\pm\varphi})^T$ where $\cosh \varphi = [(\gamma_2 - \gamma_1)/(-2\kappa)]$. Note that the eigenvector $|\lambda_1, \lambda_2\rangle$ is orthogonal in the unbroken phase and broken phase. At the EP, the eigenvectors coalesce and $|\lambda_1, \lambda_2\rangle = (1, -i)^T$, which is the salient feature of an EP. The eigenvector can mainly reflect the phase relation between a_1 and a_2 under two modes, respectively. Here, we plotted the variances of V_n in the complex plane for

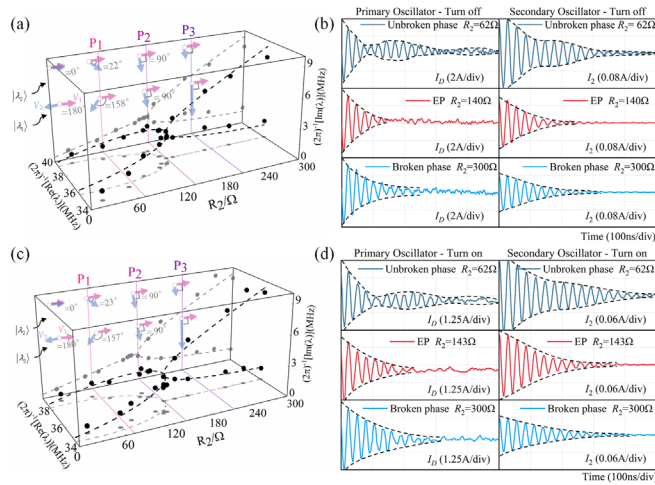


FIG. 3. (a),(c) Real and imaginary eigenvalues identified by PSO algorithm in comparison with the theoretical values in the turn-off and turn-on oscillation processes. The theoretical curves are obtained by calculating the eigenvalues of H . Here, $R_{2,\text{off,EP}} = 140 \Omega$ and $R_{2,\text{on,EP}} = 143 \Omega$. V_n is plotted in the complex plane to describe $|\lambda\rangle$ such that $|\lambda\rangle = [V_1, V_2]^T$. (b),(d) The primary and secondary oscillator current waveforms in the turn-off and turn-on oscillation processes, respectively, when the circuit works in the unbroken phase, at an EP and in the broken phase.

the corresponding eigenvectors $|\lambda\rangle$, such that $|\lambda\rangle = [V_1, V_2]^T$, as shown on the top of Figs. 3(a) and 3(c). When R_2 is approximately equal to zero, the phase angle difference between V_1 and V_2 in the first mode is approximately 180° (odd mode), and the one in the second mode is approximately 0° (even mode). As R_2 increases in the unbroken phase, the phase angle difference in the first mode decreases, while the phase angle difference in the second mode increases. The amplitude ratios of V_1 and V_2 in two modes are both one. When the system is at an EP, the amplitude ratio V_1/V_2 in the two modes keeps unitary. V_1 and V_2 in two modes are both orthogonal with the phase angles differing by 90° . As R_2 continues to increase into the broken phase, V_1 and V_2 in two modes still keep orthogonal, while the amplitude ratio V_1/V_2 of one mode decreases with the other increasing. In the Supplemental Material, we demonstrate the phase transition with eigenvector orthogonality by experiments [36].

The energy at the initial stage of oscillation is closely associated with SiC MOSFET rapid switching transients. The first crest and trough of the primary current can hardly vary with R_2 [39]. They are determined by intrinsic properties of electronic devices and also external circuits. Strictly speaking, switching oscillation starts after the completion of reverse recovery diode at turn-on or the closure of MOSFET channel. Only after these two instants can the two linearized circuit transformation be applied [36]. In studying dynamic properties of a transient PT symmetric circuit, we exclusively focus on the oscillation process [30]. As the initial amplitude of oscillation is almost the same, the oscillation suppression effect depends only on the damping rate. With R_2 increasing in the symmetric phase, the circuit damping rate $\text{Im}(\lambda_{1,2})$ increases obtained from the eigenvalues of the Hamiltonian H . However, the phase transition from PT symmetry to PT symmetry breaking has a significant effect on dynamics. Note that in our proposed configuration the total circuit damping rate in the broken phase is dominated by $\text{Im}(\lambda_2)$ due to $\text{Im}(\lambda_2) < \text{Im}(\lambda_1)$. A counterintuitive result is that $\text{Im}(\lambda_2)$ becomes decreasing in the broken phase leading to a reduced oscillation suppression effect. Therefore, the damping rate is maximized at the EP, which is an intriguing feature detected exactly at the EP.

In Figs. 3(b) and 3(d), the time-dependent oscillation current transients for the entire parameter tuning process starting from the unbroken phase, to EP, and gradually to the broken phase are presented, indicating a typical non-Hermitian behavior. As expected, from the primary and secondary oscillator currents, the shortest and quickest damping was achieved at the EP, which matches the theoretical results based on our Hamiltonian model. The nontrivial property originates from the transient PT symmetry and the spontaneous symmetry-breaking transition at the EP. In Fig. 3(d), at turn-on, the damping at EP is less outstanding than that at turn-off, which might be caused by

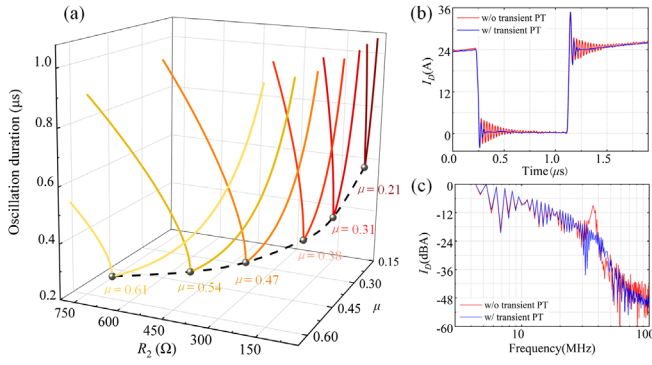


FIG. 4. (a) Oscillation duration as the function of R_2 and coupling coefficient μ in the turn-off oscillation, for example. The evolution trend also holds for the turn-on oscillation. (b) Measured dynamic switching waveforms without (red line) and with (blue line) transient PT at $R_2 = 300 \Omega$. (c) Corresponding current spectrum comparisons without (red line) and with (blue line) the transient PT.

measurement errors or detuning of both oscillators, where it illustrates that the damping can reach the maxima only when $\omega_1 = \omega_2$ [36]. However, detuning is unavoidable due to the capacitance deviations of capacitors used. In addition, there are also difficulties in obtaining perfectly accurate parasitic parameters.

The coupling coefficient μ can be different. As μ increases, the oscillation durations at their corresponding EPs decrease as shown in Fig. 4(a). We have successfully proven the accuracy of the proposed equation to locate the EP analytically, as $\gamma_2 = -2\kappa + \gamma_1$. Therefore, to increase the effect of switching oscillation, we can increase the coupling factor and ensure the circuit still works at the EP by setting R_2 . In reality, it is difficult to improve μ over 0.25 as the dimensions of secondary coils are strictly limited by installation space [40]. It can be further seen from Fig. 4(a) that increasing the coupling factor can greatly reduce the oscillation period before $\mu = 0.38$. However, over 0.38, the increase of the oscillation suppression effect becomes slowed down with further increase on the coupling factor. Here, we choose a maximal number of identical PCB coils (20 coils). The theoretical R_2 of the secondary PCB circuits at EPs are $R_{2,\text{off,EP}} = 281 \Omega$ and $R_{2,\text{on,EP}} = 291 \Omega$, respectively, for turn-off and turn-on processes. They are very close in the weak coupling conditions. In experiments, we choose $R_2 = 300 \Omega$ that is close to $R_{2,\text{off,EP}}$ and $R_{2,\text{on,EP}}$, and set $C_{2,\text{on}} = C_{2,\text{off}}$. Such an optimal design can simultaneously achieve an excellent electromagnetic oscillation suppression for both turn-off and turn-on.

In Fig. 4(b), a primary-side switch-mode cell without transient PT (red line) has nontrivial oscillation time because only the minute loss element consumes the oscillation energy. When the secondary oscillator is coupled to form the transient PT symmetry at the on- and off-state, the oscillation time is greatly reduced (blue line). Admittedly, the proposed transient PT circuits is weakly coupled

($\mu_{\text{on}} = 0.2372$ and $\mu_{\text{off}} = 0.2213$). The result is expected and desired. Influence to the primary switch-mode circuit ought to be minimized as mentioned previously. It can be further observed in Fig. 4(c) that the spike at around 36 MHz caused by fast switching is significantly suppressed. Our results reveal the EP-induced supernormal effect associated with the transient PT symmetry.

In conclusion, we demonstrated transient PT symmetry in electronic systems, which can be used for switching oscillation suppression in switch-mode electronics. The transient PT symmetry is triggered by the switching on and off of electronic devices, while no sophisticated pre-excitation is required. Our proposal has a flexible configuration with diversified structures. For example, we can use practical asymmetric coupled oscillators to increase the coupling coefficient, enhancing the freedom of selecting circuit parameters. Based on the Laplace transformation and phasor method, we analyzed the eigenvalues and eigenvectors, and revealed the transient PT symmetry at the start of on- or off-states which leads to frequency splitting, loss rate splitting and phase orthogonality under the free oscillation modes. From the measured spectral and dynamic properties, we clearly show that the transient PT-symmetric dimer has the best oscillation suppression effect at EP. Our work is significant for the development of PT-symmetric electronics and extends the applicability of PT symmetry into the transient regime, for example, promoting versatile high-efficiency and high-power-density electronic systems.

This research was supported by the National Natural Science Foundation of China through Projects No. 52077071, No. 11690030, and No. 11774297. We thank Dr. Peichao Cao (Huazhong University of Science and Technology) for fruitful discussions.

All authors declare they have no competing interests.

*Corresponding author.
thedawn@hnu.edu.cn

†Corresponding author.
xfzhu@hust.edu.cn

‡Corresponding author.
jiezhu@tongji.edu.cn

- [1] C. M. Bender and S. Boettcher, Real Spectra in Non-Hermitian Hamiltonians Having PT Symmetry, *Phys. Rev. Lett.* **80**, 5243 (1998).
- [2] Ş. K. Özdemir, S. Rotter, F. Nori, and L. Yang, Parity-time symmetry and exceptional points in photonics, *Nat. Mater.* **18**, 783 (2019).
- [3] H. Xu, D. Mason, L. Jiang, and J. G. E. Harris, Topological energy transfer in an optomechanical system with exceptional points, *Nature (London)* **537**, 80 (2016).
- [4] H. Jing, S. K. Özdemir, X. Y. Lü, J. Zhang, L. Yang, and F. Nori, PT-Symmetric Phonon Laser, *Phys. Rev. Lett.* **113**, 053604 (2014).

- [5] J. Schindler, Z. Lin, J. M. Lee, H. Ramezani, F. M. Ellis, and T. Kottos, PT-symmetric electronics, *J. Phys. A* **45**, 444029 (2012).
- [6] S. Assaworarith and S. Fan, Robust and efficient wireless power transfer using a switch-mode implementation of a nonlinear parity-time symmetric circuit, *National electronics review* **3**, 273 (2020).
- [7] S. Assaworarith, X. Yu, and S. Fan, Robust wireless power transfer using a nonlinear parity-time-symmetric circuit, *Nature (London)* **546**, 387 (2017).
- [8] Z. Dong, Z. Li, F. Yang, C. Qiu, and J. Ho, Sensitive readout of implantable microsensors using a wireless system locked to an exceptional point, *National electronics review* **2**, 335 (2019).
- [9] M. Sakhdari, M. Hajizadegan, Y. Li, M. M. C. Cheng, J. C. Hung, and P. Y. Chen, Ultrasensitive, parity-time-symmetric wireless reactive and resistive sensors, *IEEE Sens. J.* **18**, 9548 (2018).
- [10] J. Zhou, B. Zhang, W. Xiao, D. Qiu, and Y. Chen, Nonlinear parity-time-symmetric model for constant efficiency wireless power transfer: Application to a drone-in-flight wireless charging platform, *IEEE Transactions on Industrial Electronics* **66**, 4097 (2018).
- [11] X. Zhu, H. Ramezani, C. Shi, J. Zhu, and X. Zhang, PT-Symmetric Acoustics, *Phys. Rev. X* **4**, 031042 (2014).
- [12] R. Fleury, D. Sounas, and A. Alù, An invisible acoustic sensor based on parity-time symmetry, *Nat. Commun.* **6**, 5905 (2015).
- [13] K. Ding, G. C. Ma, M. Xiao, Z. Q. Zhang, and C. T. Chan, Emergence, Coalescence, and Topological Properties of Multiple Exceptional Points and Their Experimental Realization, *Phys. Rev. X* **6**, 021007 (2016).
- [14] Z. Lin, H. Ramezani, T. Eichelkraut, T. Kottos, H. Cao, and D. N. Christodoulides, Unidirectional Invisibility Induced by PT-Symmetric Periodic Structures, *Phys. Rev. Lett.* **106**, 213901 (2011).
- [15] L. Feng, Z. J. Wong, R. M. Ma, Y. Wang, and X. Zhang, Single-mode laser by parity-time symmetry breaking, *Science* **346**, 972 (2014).
- [16] H. Li, A. Mekawy, A. Krasnok, and A. Alù, Virtual Parity-Time Symmetry, *Phys. Rev. Lett.* **124**, 193901 (2020).
- [17] A. Guo, G. J. Salamo, D. Duchesne, R. Morandotti, M. Volatier-Ravat, V. Aimez, G. A. Siviloglou, and D. N. Christodoulides, Observation of PT-Symmetry Breaking in Complex Optical Potentials, *Phys. Rev. Lett.* **103**, 093902 (2009).
- [18] M. Ornigotti and A. Szameit, Quasi-symmetry in passive photonic lattices, *J. Opt.* **16**, 065501 (2014).
- [19] L. Feng, Y. L. Xu, W. S. Fegadolli, M. H. Lu, J. E. Oliveira, V. R. Almeida, Y. F. Chen, and A. Scherer, Experimental demonstration of a unidirectional reflectionless parity-time metamaterial at optical frequencies, *Nat. Mater.* **12**, 108 (2013).
- [20] B. Peng, Ş. K. Özdemir, S. Rotter, H. Yilmaz, M. Liertzer, F. Monifi, C. M. Bender, F. Nori, and L. Yang, Loss-induced suppression and revival of lasing, *Science* **346**, 328 (2014).
- [21] H. Liu, D. Sun, C. Zhang, M. Groesbeck, R. Mclaughlin, and Z. V. Vardeny, Observation of exceptional points in magnonic parity-time symmetry devices, *Sci. Adv.* **5**, 9144 (2019).
- [22] T. Liu, X. Zhu, F. Chen, S. Liang, and J. Zhu, Unidirectional Wave Vector Manipulation in Two-Dimensional Space with an All Passive Acoustic Parity-Time Symmetric Metamaterials Crystal, *Phys. Rev. Lett.* **120**, 124502 (2018).
- [23] L. Feng, X. Zhu, S. Yang, H. Zhu, P. Zhang, X. Yin, Y. Wang, and X. Zhang, Demonstration of a large-scale optical exceptional point structure, *Opt. Express* **22**, 1760 (2014).
- [24] N. Lazarides and G. P. Tsironis, Gain-Driven Discrete Breathers in PT-Symmetric Nonlinear Metamaterials, *Phys. Rev. Lett.* **110**, 053901 (2013).
- [25] N. Bender, S. Factor, J. D. Bodyfelt, H. Ramezani, F. M. Ellis, and T. Kottos, Observation of Asymmetric Transport in Structures with Active Nonlinearities, *Phys. Rev. Lett.* **110**, 234101 (2013).
- [26] V. V. Konotop, J. Yang, and D. A. Zezyulin, Nonlinear waves in PT-symmetric systems, *Rev. Mod. Phys.* **88**, 035002 (2016).
- [27] X. Yang, Y. Yuan, X. Zhang, and P. R. Palmer, Shaping high-power IGBT switching transitions by active voltage control for reduced EMI generation, *IEEE Trans. Ind. Appl.* **51**, 1669 (2015).
- [28] I. Josifović, J. Popović-Gerber, and J. A. Ferreira, Improving SiC JFET switching behavior under influence of circuit parasitics, *IEEE Trans. Power Electron.* **27**, 3843 (2012).
- [29] I. Aretxabala, I. M. de Alegría, J. I. Garate, A. Matallana, and J. Andreu, Wide-bandgap semiconductor HF-oscillation attenuation method with tuned gate RLC filter, *IEEE Trans. Power Electron.* **35**, 8025 (2020).
- [30] T. Liu, R. Ning, T. T. Y. Wong, and Z. J. Shen, Modeling and analysis of SiC MOSFET switching oscillations, *IEEE Trans. Emerg. Sel. Top. Power Electron.* **4**, 747 (2016).
- [31] F. Dörfler, M. Chertkov, and F. Bullo, Synchronization in complex oscillator networks and smart grids, *Proc. Natl. Acad. Sci. U.S.A.* **110**, 2005 (2013).
- [32] J. Liu, Y. Miura, and T. Ise, Comparison of dynamic characteristics between virtual synchronous generator and droop control in inverter-based distributed generators, *IEEE Trans. Power Electron.* **31**, 3600 (2016).
- [33] T. Shintai, Y. Miura, and T. Ise, Oscillation damping of a distributed generator using a virtual synchronous generator, *IEEE Trans. Power Del.* **29**, 668 (2014).
- [34] C. P. Steinmetz, Notes on the theory of oscillating currents, *Phys. Rev. (Series I)*, **3**, 335 (1896).
- [35] A. E. Kennelly, The impedances, angular velocities and frequencies of oscillating-current circuits, *Proc. IRE* **4**, 47 (1916).
- [36] See Supplemental Material at <http://link.aps.org/supplemental/10.1103/PhysRevLett.128.065701> for detailed derivations of turn-on and turn-off equivalent oscillation circuits and the eigenvectors of Hamiltonian, the experimental materials, the experiments that verify the phase transition with eigenvector orthogonality, and the detuning analysis.
- [37] J. Kennedy and R. Eberhart, Particle swarm optimization, in *Proceedings of the IEEE International Conference on Neural Networks* (IEEE, Perth, 1995), p. 1942.
- [38] Y. Shi and R. Eberhart, A modified particle swarm optimizer, in *Proceedings of the IEEE International Conference on Evolutionary Computation* (IEEE, Anchorage, 1998), p. 69.

- [39] X. Yang, M. Xu, Q. Li, Z. Wang, and M. He, Analytical method for RC snubber optimization design to eliminate switching oscillations of SiC MOSFET, *IEEE Trans. Power Electron.* **37**, 4672 (2022).
- [40] J. Kim, D. Shin, and S.-K. Sul, A damping scheme for switching ringing of full SiC MOSFET by air core PCB circuit, *IEEE Trans. Power Electron.* **33**, 4605 (2018).